

STABILITY PROPERTIES OF MAGNETIC TOWER JETS

MASANORI NAKAMURA¹, HUI LI¹, AND SHENGTAI LI²

Draft Version August 31, 2006: Submitted to ApJ

ABSTRACT

Stability properties of “magnetic tower” jets propagating in the gravitationally stratified background have been examined by performing three-dimensional magnetohydrodynamic simulations. The current-carrying, Poynting flux-dominated magnetic tower jet, which possesses a highly wound helical magnetic field, is subject to the current-driven instability (CDI). We find that, under general physical conditions including small perturbations in the initial background profiles, the propagating magnetic tower jets develop the non-axisymmetric, $m = 1$ kink mode of the CDI. The kink mode grows on the local Alfvén crossing time scale. In addition, two types of kink modes appear in the system. At the central region where external thermal pressure confinement is strong, only the internal kink mode is excited and will grow. A large distance away from the central region where the external thermal pressure becomes low, the external kink mode is observed. As a result, the exterior of magnetic tower jets will be deformed into a large-scale wiggled structure. We also discuss extensively the different physical processes that contribute to the overall stability properties of the magnetic tower jets. Specifically, when the jet propagates in an initially unperturbed background, we find that they can survive the kink mode beyond the point predicted by the well-known Kruskal-Shafranov (K-S) criterion. The stabilization in this case comes mainly from the dynamical relaxation of magnetic twists during the propagation of magnetic towers; the magnetic pitch is reduced and the corresponding K-S critical wavelength becomes longer as the tower jet proceeds. Furthermore, we show that the pressure-driven and Kelvin-Helmholtz instabilities do not occur in the magnetic tower jets. This strongly suggests that the CDI is the primary reason for the wiggling structures in jets.

Subject headings: instabilities — galaxies: active — galaxies: jets — methods: numerical — MHD

1. INTRODUCTION

Magnetohydrodynamic (MHD) mechanisms are often invoked to explain the launching, acceleration and collimation of jets from Young Stellar Objects, X-ray binaries, Active Galactic Nuclei (AGNs), Microquasars, and Quasars (see, *e.g.*, Meier et al. 2001, and references therein). Strongly magnetized jets, particularly those with a strong toroidal field encircling the collimated flow, are often referred to as “current-carrying” or “Poynting flux-dominated” (PFD) jets. A large current flowing parallel to the jet flow is responsible for generating a strong, tightly wound helical magnetic field. The global picture of a current-carrying jet with a closed current system linking the magnetosphere of the central engine and the hot spots was introduced by Benford (1978, 2006) and applied to AGN double radio sources. This closed current system includes a pair of current circuits, each containing both a forward electric current path (the jet flow itself, with its toroidal magnetic field, toward the lobe), and a return electric current path (along some path back to the AGN core).

Recent high resolution observations, in X-ray, optical and radio bands, show that many AGN and quasar jets display wiggles/kinks, which may be associated with a helical motion of the underlying bulk flow, in wide spatial ranges from sub-parsec to kpc scales (*e.g.*, Reid et al. 1989; Hummel et al. 1992; Baum et al. 1997; Feretti et al. 1999; Lobanov & Zensus 2001; Marshall et al. 2001; Eilek & Owen 2002; Savolainen et al. 2006). Many ideas have been proposed for these helical distortions: MHD instabilities such as the Kelvin-Helmholtz instability (KHI),

the current-driven instability (CDI), and the pressure-driven instability (PDI), or the precession of the jet ejection axis due to the existence of a binary black hole (Begelman et al. 1980), or an encounter with another galactic core.

It is well known that a cylindrical plasma column with a helical magnetic configuration is subject to the $m = 0$ (sausage) mode of PDI, the $m = 1$ (kink) mode of CDI, and the other higher order modes, where m is the azimuthal (ϕ) mode number (see, *e.g.*, Kadomtsev 1966; Bateman 1978; Freidberg 1982, for details). CDI is driven by parallel (axial) current flows and can exist even in a zero pressure, force-free plasma. On the other hand, PDI is powered by perpendicular current flows and it is often known as the interchange (internal) modes. KHI is considered to be very important at the shearing boundary between the flowing jet and the external medium, particularly in the kinetic flux-dominated (KFD) jets. In principle, CDI and KHI have both external (surface) and internal (body) modes. PFD jets should be especially susceptible to CDI rather than PDI and KHI. This is because the strong axial electric current is present inside the PFD jets, which is responsible for the highly wound helical field configurations, and the Lorentz force plays an important role in the jet dynamics. The investigation of the destructive influence of CDI on PFD jet flows is an important avenue of research in the study of astrophysical jets.

Much more attention on studies of stabilities (disruption of the interior/exterior of astrophysical jets) have given to KHI than to CDI. This is because jets were believed to be super-Alfvénic or super-fast magnetosonic KFD flows (*i.e.*, kinetic energy was expected to greatly exceed the magnetic energy). However, it is not necessarily always the case; a super-Alfvénic or super-fast magnetosonic PFD flow can exist in both nonrelativistic (Kudoh & Shibata 1997; Vlahakis et al. 2000) and relativistic (Vlahakis & Königl 2001) MHD out-

¹ Theoretical Astrophysics, MS B227, Los Alamos National Laboratory, NM 87545; nakamura@lanl.gov

² Mathematical Modeling and Analysis, MS B284, Los Alamos National Laboratory, NM 87545

flow solutions. Analytic studies on the CDI as a possible explanation for jet disruption have been performed as well (Eichler 1993; Spruit, Foglizzo, & Stehle 1997; Begelman 1998; Lyubarskii 1999). Linear analyses of nonrelativistic force-free jets, which are thermally confined by the external nonmagnetized medium, were performed in super-fast (Appl & Camenzind 1992) or trans-fast (Appl 1996) magnetosonic regimes. They found that the growth rate of CDI is always substantially smaller than those of KHI in their specific treatment. Only for quite small fast magnetosonic numbers, $M_F \lesssim 0.5$, both become comparable. Linear analyses of the relativistic force-free jets, in case of constant-longitudinal field B_z along the jet axis, were performed by Istomin & Pariev (1994, 1996). They concluded that such a jet is stable against CDI, while Lyubarskii (1999) analyzed the relativistic force-free jets with B_z decreasing outwards and found that they are unstable.

Nonlinear development of the CDI for cold super-fast magnetosonic jets has been studied by Lery et al. (2000), based on the linear analysis (Appl et al. 2000). It was found that the current density is redistributed within the inner part of the jet radius on a characteristic time scale of the order of the Alfvén crossing time in the jet frame. Nothing in their numerical results indicated a possible disruption of the jet by the CDI sausage ($m = 0$) or kink ($m = 1$) modes (see also Lery & Frank 2000; Frank et al. 2000). In general, these linear/nonlinear considerations conclude that “current-driven instabilities are unlikely to be dangerous for the integrity of astrophysical jets” (Appl 1996) and this has been widely accepted in theoretical/observational communities. In the nonlinear regime, an interplay between KHI and CDI can occur in the helically magnetized flow even with slightly super-fast magnetosonic speed $M_F \gtrsim 1$ (Baty & Keppens 2002). This nonlinear interaction can contribute to jet survival, and the large-scale magnetic deformations associated with the CDI mode development can effectively saturate KHI surface vortices and prevent jet disruption.

By contrast, the first attempt to investigate the nonlinear behavior of visible distortion in KFD jets along the large-scale magnetic field by the CDI kink mode was performed by Todo et al. (1993) to model Herbig Haro objects. In a similar study, Nakamura et al. (2001) examined the formation of wiggled structures by the $m = 1$ mode in PFD jets to apply for AGN jets. Their numerical result is applicable for the systematic distribution of the observed rotation measure in 3C 449 (Feretti et al. 1999), associated with the jet deformation (Kigure et al. 2004). The rotating PFD/KFD jets can be potentially stabilized against the $m = 1$ mode beyond the original Kruskal-Shafranov criterion, however, sudden destabilization of rotating jets due to the $m = 1$ mode can occur via the angular momentum loss triggered by MHD shock waves (Nakamura & Meier 2004).

The purpose of the present paper is to discuss the stability properties of “magnetic tower” jets, which have not been studied in the past work. Of particular interest here is the nonlinear growth of the CDI kink mode. The CDI kink mode in magnetic tower jets may be distinguished from that in the classical MHD jets along the large-scale magnetic field (Todo et al. 1993; Nakamura et al. 2001; Nakamura & Meier 2004), while it should be comparable directly to “non-disrupting” models (Appl 1996; Appl et al. 2000; Lery et al. 2000), in which the MHD jets are assumed to be in pressure equilibrium with an unmagnetized ambient medium.

This is the third of our series of papers to examine the nonlinear magnetic tower jets. The first of our series, Li et al. (2006, hereafter Paper I), described the basic assumptions and the approaches in the numerical modeling of magnetic tower jets. The evolution of the tower jets in a constant density/pressure background has been examined there. The second of our series, Nakamura et al. (2006, hereafter Paper II) investigated the global structure of magnetic tower jets in the gravitationally stratified atmosphere (a more realistic astrophysical situation), in terms of the MHD waves structure, the radial force equilibrium, and the collimation. In the present paper, the third of our series, we investigate the stability properties of magnetic tower jets. We examine our numerical results in two cases; one without initial perturbations and another with initial perturbations. The former exhibits the quasi-axisymmetric evolution without any growth of MHD instabilities, while the latter shows non-axisymmetric evolution by the CDI modes. This paper is organized as follows. In §2, we outline our numerical methods. In §3, we describe our numerical results. Discussion and conclusion are given in §4 and §5.

2. NUMERICAL METHODS AND MODEL ASSUMPTIONS

We solve the nonlinear system of time-dependent ideal MHD equations numerically in a 3-D Cartesian coordinate system (x, y, z) . The basic numerical treatments (including the MHD numerical scheme) is essentially the same as that in Paper I and II. We assume an initial hydrostatic equilibrium in the gravitationally stratified medium, adopting an iso-thermal King model (King 1962). The magnetic flux and the mass are steadily injected in a central small volume during a certain time period. Since the injected magnetic fields are not force-free, they will evolve as a “magnetic tower” and interact with the ambient medium.

2.1. Numerical Set Up

In this paper, we present mainly two different cases: one is called the “unperturbed case” in the following discussion, which is a run without any initial perturbation to the background initial profiles. This simulation is taken from the run presented in Paper II. The other is called the “perturbed case”, where a finite amplitude perturbation (a few percent of the background sound speed) is given to the velocities of the background gas.

The total computational domain is taken to be $|x|, |y|, |z| \leq 16$. The numbers of grid points in the simulations reported here are 240^3 in the unperturbed case and 320^3 in the perturbed case, where the grid points are assigned uniformly in the x, y , and z directions. We normalize physical quantities with the unit length scale R_0 , the unit density ρ_0 , the sound speed C_{s0} as the typical velocity field in the system, and other quantities derived from their combinations, e.g., the typical time t_0 as R_0/C_{s0} , etc. Normalizing factors are $R_0 = 5$ kpc, $C_{s0} = 4.6 \times 10^7$ cm/s, $t_0 = 1.0 \times 10^7$ yrs, $\rho_0 = 5.0 \times 10^{-27}$ g/cm³, the unit pressure p_0 as $\rho_0 C_{s0}^2 = 1.4 \times 10^{-11}$ dyn/cm², and the unit magnetic field B_0 as $\sqrt{4\pi\rho_0 C_{s0}^2} = 17.1$ μ G. We take ρ_0 and p_0 as the initial quantities at the origin $(x, y, z) = (0, 0, 0)$ and the ρ and p at the origin in the simulations are set to unity. The initial sound speed in the simulation is constant, $C_s = \gamma^{1/2} \approx 1.29$, throughout the computational domain. The simulation domain is from -80 to 80 kpc, with $\Delta x = \Delta y = \Delta z \sim 0.13$ for the unperturbed case and $\Delta x = \Delta y = \Delta z \sim 0.1$ for

the perturbed case, which correspond to ~ 0.67 kpc and ~ 0.5 kpc respectively. An important time scale in the system is the sound crossing time $\tau_s \approx 0.78$, corresponding to a typical time scale $R_0/C_{s0} \approx 10.0$ Myrs. Therefore, $t = 1$ is equivalent to the unit time scale 12.8 Myrs.

In the King model we use here, we adopt the cluster core radius R_c to be 4.0 (i.e., 20 kpc) and the slope κ to be 1.0 in the unperturbed case and 0.75 in the perturbed case. The injections of magnetic flux, mass and its associated energies are the same as those described in Paper I. The ratio between the toroidal to poloidal fluxes of the injected fields is characterized by a parameter $\alpha = 15$, which corresponds to ~ 6 times more toroidal flux than poloidal flux. The magnetic field injection rate is described by γ_b and is set to be $\gamma_b = 3$. The mass is injected at a rate of $\gamma_\rho = 0.1$ over a central volume with a characteristic radius $r_\rho = 0.5$. Magnetic fluxes and mass are continuously injected for $t_{\text{inj}} = 3.1$, after which the injection is turned off. These parameters correspond to a magnetic energy injection rate of $\sim 10^{43}$ ergs/s, a mass injection rate of $\sim 0.046 M_\odot/\text{yr}$, and an injection time ~ 40 Myrs. We use the outflow boundary conditions at all outer boundaries. Note that for most of the simulation duration, the waves and magnetic fields stay within the simulation box, and all magnetic fields are self-sustained by their internal currents.

2.2. Definition of Forward and Return Currents

As examined in Paper II, the magnetic tower jets can propagate without any visible distortion throughout the time evolution (see Fig. 1 of Paper II). The magnetic tower has a well-ordered helical magnetic configuration; a tightly wound central helix is going up inside the tower jet and a loosely wound helix is coming back at the outer edge of magnetic tower jet (see Fig. 3 of Paper II). The axial current flow J_z displays a closed circulating current system in which one path flows along the central axis (the ‘‘forward’’ current) and another conically shaped path that flows outside (the ‘‘return’’ current) (see Fig. 4 of Paper II). Here, we define the forward current density \mathbf{J}^F and the return current density \mathbf{J}^R as follows;

$$\mathbf{J} \equiv \begin{cases} \mathbf{J}^F & (J_z > 0) \\ \mathbf{J}^R & (J_z < 0) \end{cases}. \quad (1)$$

Note that \mathbf{J}^F (and \mathbf{J}^R) is a vector and can have additional radial and azimuthal components J_r^F and J_ϕ^F (J_r^R and J_ϕ^R) with any sign.

2.3. The Kruskal-Shafranov Criterion

According to the well-known Kruskal-Shafranov (K-S) criterion (Shafranov 1957; Kruskal et al. 1958), a magnetized flux tube (along the z axis) is stable to the kink ($m = 1$) mode as long as the magnetic twist angle $\Phi(r)$ is below some critical value Φ_{crit} ,

$$\Phi(r) \equiv \frac{LB_\phi}{rB_z} < \Phi_{\text{crit}}, \quad (2)$$

where, L is the length of the current-carrying magnetic flux system, r is the cylindrical radius of the flux tube, and B_z and B_ϕ are the axial and azimuthal field components in a cylindrical coordinate, respectively. In the original K-S criterion, Φ_{crit} is equal to 2π . The effect of ‘‘line-tying’’, i.e., fixing the radial motion of the magnetic fluxes at the boundary, however, could raise the stability threshold. (In the solar coronal loops, the foot points of magnetic fluxes can be anchored in a high density region as chromosphere.) The modified critical

values for a force-free magnetic loop configuration in solar coronal loops are between 2π and 10π (e.g., Hood & Priest 1979; Einaudi & Van Hoven 1983). For the configuration of an astrophysical jet, which has $L \gg r$, inequality (2) can be easily violated. If the MHD jets originate from an accretion disk, the bottom part of jets may be line-tied in the disk and the top part of jets can be free against the radial motion; i.e., a ‘‘semi’’ line-tying configuration. (Further argument of the stabilizing effect by semi line-tying will be presented in §4.2.) For lack of detailed linear analysis of ‘‘semi’’ line-tying magnetic configurations, we still define $\Phi_{\text{crit}} = 2\pi$, which should only be regarded as a guide for gauging the stability, rather than a precise threshold. Here, we replace L by a spectrum of axial wavelengths λ , and define the critical wavelength to be the one that is marginally stable:

$$\lambda_{\text{crit}} \equiv \frac{\Phi_{\text{crit}} r B_z}{B_\phi} = \frac{2\pi r B_z}{B_\phi}. \quad (3)$$

The K-S stability criterion (eq. [2]) then becomes

$$\lambda < \lambda_{\text{crit}}, \quad (4)$$

so that wavelengths greater than λ_{crit} could be unstable to the CDI kink mode.

2.4. Diagnostics of Non-axisymmetric Mode

To better diagnose the non-axisymmetric distortion, we perform the power spectrum analysis of the magnitude of the current density $|\mathbf{J}|$. We analyze the modal structure of $|\mathbf{J}|$ by performing the volume-averaged Fourier transform:

$$f(m, k) = \frac{1}{V_{\text{cl}}} \int \int \int_{V_{\text{cl}}} |\mathbf{J}| e^{i(m\phi + kz)} r dr d\phi dz, \quad (5)$$

where $|\mathbf{J}| \equiv (J_r^2 + J_\phi^2 + J_z^2)^{1/2}$ and V_{cl} is the cylindrical volume that encloses $\mathbf{J} (\equiv \mathbf{J}^F + \mathbf{J}^R)$

$$V_{\text{cl}} = \int_{r_a}^{r_b} \int_0^{2\pi} \int_{z_a}^{z_b} r dr d\phi dz. \quad (6)$$

We use the values $r_a = 0.0$, $r_b = 7.75$, $z_a = 0.0$, and $z_b = 15.5$ in the ‘‘upper’’ volume and use $z_a = -15.5$ and $z_b = 0.0$ in the ‘‘lower’’ volume. The quantity $f(m, k)$ is a function of the azimuthal mode number m and axial wave number $k = 2\pi/\lambda$ (corresponding to a characteristic wave length λ), and it is a function of time as well.

Finally, we identify the power spectrum as

$$|f(m, k)|^2 = \{\text{Re}[f(m, k)]\}^2 + \{\text{Im}[f(m, k)]\}^2, \quad (7)$$

$$\begin{aligned} \text{Re}[f(m, k)] &= \frac{1}{V_{\text{cl}}} \int \int \int_{V_{\text{cl}}} |\mathbf{J}| \cos(m\phi + kz) r dr d\phi dz, \quad (8) \end{aligned}$$

$$\begin{aligned} \text{Im}[f(m, k)] &= \frac{1}{V_{\text{cl}}} \int \int \int_{V_{\text{cl}}} |\mathbf{J}| \sin(m\phi + kz) r dr d\phi dz. \quad (9) \end{aligned}$$

We will examine the time-dependent behavior of the power spectrum and the growth of each mode.

3. RESULTS

3.1. *Unperturbed Case — Dynamical Stabilization against the CDI Kink Mode*

We first re-examine the numerical result of Paper II as an unperturbed case, from a viewpoint of stability. For that simulation, we did not impose any initial perturbations to the background state. So the only available perturbations are from the numerical noise in the double precision computations. Figure 1 shows the snapshots of J_z (*top*) and λ_{crit} (*bottom*) in the final stage ($t = 10.0$). Again, we can identify the circulating path of axial current flow J_z which consists of both the forward axial current density J_z^{F} ($J_z > 0$) and the return current J_z^{R} ($J_z < 0$) in the *top* panel (J_z^{F} lies around the central axis, while J_z^{R} surrounds J_z^{F}). The maximum strength of $|J_z^{\text{F}}|$ is much larger than that of $|J_z^{\text{R}}|$, indicating that a tightly wound central helix is going up at the center of the tower and a loosely wound helix is coming back at the tower edge. The paths of forward and return currents are approaching one another around the mid-plane $|z| \lesssim 4.0$. On the other hand, the path of return current is radially expanding at the upper axial position $|z| \gtrsim 4.0$. This causes a *separation* of current flow paths in a thermally confined MHD jet with a helical magnetic field. (This plays an important role in the excitation of the external kink mode and it will be discussed in §4.3.)

As seen in the *bottom* panel, λ_{crit} has a range $2.0 \sim 6.0$ in the core part of J_z^{F} , and has no axial dependency except at the tower front. While λ_{crit} has no range in any part of J_z^{R} , meaning that the CDI kink mode is unlikely to grow at the return current region. Taking the whole part in the axial direction into consideration, the maximum length of current-carrying column is $L \sim 16$ at $t = 10.0$, which is larger than the distributed λ_{crit} in the core part of J_z^{F} . However, the non-axisymmetric displacement does not seem to occur as seen in both panels. We next show the result of the power spectrum analysis of \mathbf{J}^{F} in order to confirm the non-existence of the growing kink mode. Figure 2 shows the space-time (λ, t) diagrams of the power spectrum $|f(m, \lambda)|^2$ for $m = 1$ in the unperturbed case. We can not detect any growing non-axisymmetric mode ($m = 1$) over the wider range of axial wave length ($\lambda = 0.26 \sim 10.42$). The time variation of the power spectrum of $f(m, \lambda)$ with a selected wavelength $\lambda = 6.0$ in Fig. 3. Throughout the time evolution, the power in $m = 1$ mode is always below the axisymmetric ($m = 0$) one. Note that the variation of the $m = 0$ mode (seen in both volumes around $t = 4 \sim 8$) is due to the axisymmetric deformation of the magnetic tower into a slender-shaped structure by the gravitational contraction radially.

It may seem puzzling that, for the unperturbed case, the magnetic tower jet is stable even with $L > \lambda_{\text{crit}}$. Here, we consider a possible mechanism of the stabilizing effect in our results. Figure 4 shows the time evolution of the K-S critical wavelength λ_{crit} in the unperturbed case. A gradual increase of the distributed $\lambda_{\text{crit}} (= 2\pi r B_z / B_\phi)$ in the forward axial current-carrying column J_z^{F} can be observed. This corresponds directly to a decrease of the ratio B_ϕ / B_z . Because the injection of magnetic fluxes into the central volume in the system has been turned off at $t = 3.1$, the twisted magnetic fluxes are naturally relaxed during the expansion of the magnetic tower. The threshold length of the marginally stable of J_z^{F} in the axial (z) direction becomes longer as the magnetic tower proceeds. Therefore this “dynamical relaxation” of magnetic twists plays an important role in the stabilization

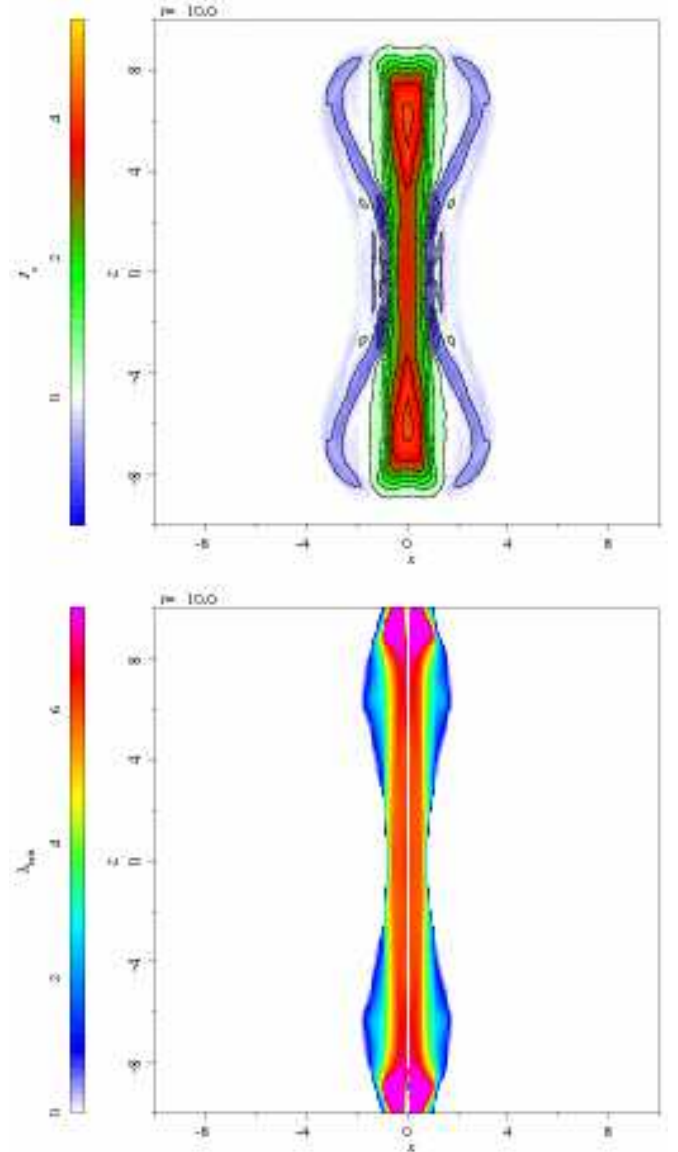


FIG. 1.— *Top*: Distribution of the axial current density J_z in the $x - z$ plane at $t = 10.0$ in the unperturbed case (Paper II). *Bottom*: Distribution of the critical wavelengths λ_{crit} at $t = 10.0$ in the $x - z$ plane, corresponding to the original Kruskal-Shafranov criterion for CDI $m = 1$ mode in the unperturbed case (Paper II).

in our current results. We will discuss other effects on the stabilization in §4.2.

3.2. *Perturbed Case — Growth of the CDI External/Internal Kink Modes*

We next examine the non-axisymmetric evolution of the magnetic tower jet in a gravitationally stratified atmosphere. To excite non-axisymmetric modes ($m \geq 1$), a small random velocity perturbation (4% of initial sound speed) has been added into the system as an initial condition.

Figure 5 shows a snapshot of the density ρ at the final stage $t = 9.5$ (see Fig. 1 of Paper II for comparison) in the perturbed case. Even though the configuration of the magnetic tower is non-axisymmetric, the main features remain similar to the unperturbed case. In general, the structure of the magnetic tower consists of both a well-collimated “body” and radially extended “lobes”. Several key features in the mag-

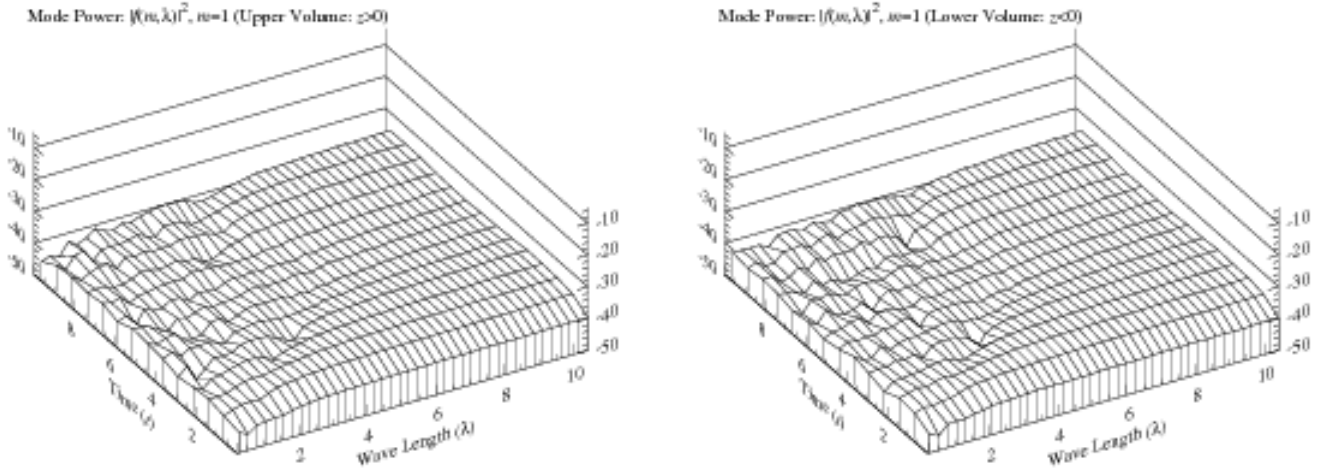


FIG. 2.— Space-time (λ, t) diagram of the azimuthal Fourier power (a natural log scale) for CDI mode $m = 1$ in the unperturbed case (Paper II). *Left*: For the upper volume $z > 0$. *Right*: For the lower volume $z < 0$.

netic tower jets (the MHD wave structures, the heating process at the tower front, the cylindrical radial force equilibrium at the tower edge, and dynamically collimating process) are the same as the unperturbed case (see Paper II for details). The Alfvén speed becomes large (about three times of local sound speed), while the plasma $\beta (\equiv 2p/B^2)$ becomes small ($\beta \lesssim 0.1$) inside the density cavities due to the expansion of magnetic fluxes. The bulk flow inside the magnetic tower is sub-sonic and sub-Alfvénic, while the fronts of the preceding hydrodynamic shock and the magnetic tower can propagate super-sonically.

Similar to Fig. 2, we present the space-time (λ, t) diagrams of the power spectrum $|f(m, \lambda)|^2$ in the perturbed case for the $m = 1$ and 2 in Fig. 6. Clearly, the growth of the $m = 1$ mode can be seen over a wide range of λ after $t \sim 4$ in both upper and lower volumes. Furthermore, the $m = 2$ (elliptical) mode also grows at a relatively short wavelength around $\lambda = 2 \sim 3$ after $t \sim 6$. To identify the growth rates of different modes, we show the time variation of the power spectrum of $f(m, \lambda)$ in the perturbed case with a selected wavelength $\lambda = 6.0$ in Fig. 7 (similar to Fig. 3). The $m = 1$ mode in both volumes exhibits an approximate exponential growth on a dynamical timescale during $t = 4 \sim 6$. At later stages, after the $m = 1$ mode grows above the axisymmetric $m = 0$ mode, its growth rate decreases slightly, but still keeps growing exponentially to saturation at the final stage. The $m = 2$ mode also shows the similar behavior with the $m = 1$ mode at the earlier stage around $t = 6 \sim 8$, but it saturates at or below the level of the $m = 0$ mode.

A linear fit using a least-square method has been performed on the initially exponential growth for the $m = 1$ mode to extract a linear growth rate

$$\text{Im}(\omega) \sim \frac{d \ln |f(m, \lambda)|^2}{dt}. \quad (10)$$

The estimated growth rates in the perturbed case are also given in Fig. 7. The growth rate in the upper volume appears to be a bit stronger than that in the lower volume. We confirm the distributed Alfvén speed V_A in the surfaces of \mathbf{J}^F is of the order of 8–9 in our normalized unit during the time evolution. The spatial length scale ξ of the non-axisymmetric ($m > 0$) distortions in the radial direction is of the order of 2–4, as seen in Fig. 5. Therefore, the inverse of the Alfvén crossing time τ_A^{-1} in the distorted part of magnetic tower jet

is given by

$$\tau_A^{-1} = \frac{V_A}{\xi} \sim 2.0 - 4.5. \quad (11)$$

This is, in general, consistent with the timescales of the growing $m = 1$ mode derived from Fig. 7. So, our results lead us to conclude that the non-axisymmetric distortion in the magnetic tower jet is caused dominantly by the normal current-driven kink ($m = 1$) mode.

Two types of CDI modes are identified in the context of magnetically controlled fusion plasma; the “external” and the “internal” modes (Bateman 1978). The external mode can be identified with a radial distortion, while in the internal mode, there is no radial perturbation at the outer edge of the current-carrying column. One of our findings in the perturbed magnetic tower jet is that the CDI external and internal modes “co-exist” during the dynamical evolution. Figure 8 shows snapshots of J_z in the perturbed case at $t = 8.0$ and 9.5. As seen in the *top* panel ($t = 8.0$), the edge of \mathbf{J}^F is clearly shifted to an offset axial direction at higher latitude ($|z| \gtrsim 4$). On the other hand, that edge never shifts non-axisymmetrically at lower latitude ($|z| \lesssim 4$). However, the non-axisymmetric distribution of \mathbf{J}^F at the inner part can be detected, indicating that the internal mode is certainly growing. At the final stage ($t = 9.5$: *bottom*), we can see the well-grown wiggles inside the “lobes”, while the edge of the “body” part in the magnetic tower still remains quasi-axisymmetric except for the inner part. Taking the result of Fig. 6 into consideration, the $m = 1$ kink mode is dominant in the external CDI at the lobes, while the $m = 2$ elliptical mode may be dominant in the internal CDI at the body of the magnetic tower. In addition, we illustrate a 3-D view of some selected magnetic lines of force in the perturbed case at the final stage $t = 9.5$ in Fig. 9. It indicates that a tightly wound central helix, which goes up along the central axis, relaxes in the lobe part where the external kink mode has taken place, and a large-scale loosely wound twist is formed there.

4. DISCUSSION

4.1. Suppression of Shear-driven Instability

We first discuss the possibility of the interplay between CDI and KHI modes in our results. The examinations of KHI in linear/nonlinear regimes have been extensively performed by P. E. Hardee and his collaborators (see, *e.g.*, Hardee 2004,

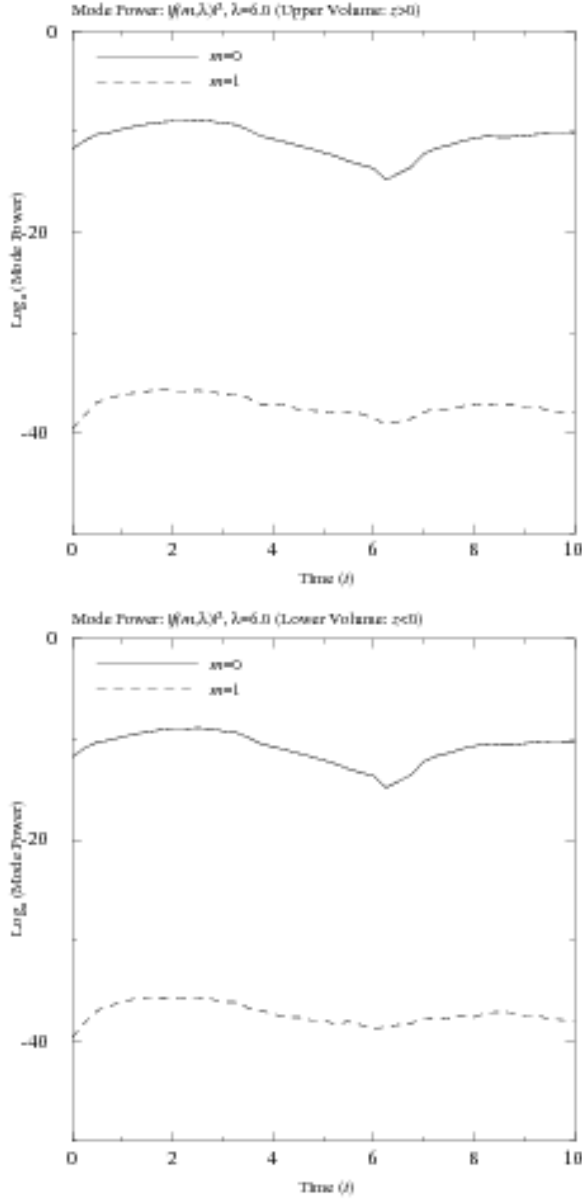


FIG. 3.— The time variation of the azimuthal Fourier power (a natural log scale) in modes $m = 0, 1$ with a specified wave length $\lambda = 6.0$ in the unperturbed case (Paper II). *Top*: For the upper volume $z > 0$. *Bottom*: For the lower volume $z < 0$.

and references therein). In general, non-axisymmetric “surface” (*external*) modes ($m > 0$) are stable against KHI for sub-Alfvénic flow. However, in super-Alfvénic but trans-fast magnetosonic flow, they can be unstable. Only axisymmetric surface mode ($m = 0$) remains unstable in sub-Alfvénic flow, although with a relatively small growth rate (Bodo et al. 1989). A potential zone of unstable region in non-axisymmetric KHI surface modes should exist in downstream of the Alfvén surface.

The instability criterion for non-axisymmetric KHI surface modes is as follows (Hardee & Rosen 2002):

$$\Delta V > V_{As} = \sqrt{\frac{\rho_j + \rho_e}{4\pi\rho_j\rho_e}(B_j^2 + B_e^2)} \quad (12)$$

where $\Delta V \equiv |V_j - V_e|$ is the velocity shear and V_{As} is the *surface* Alfvén speed (subscript j corresponds to the jet itself

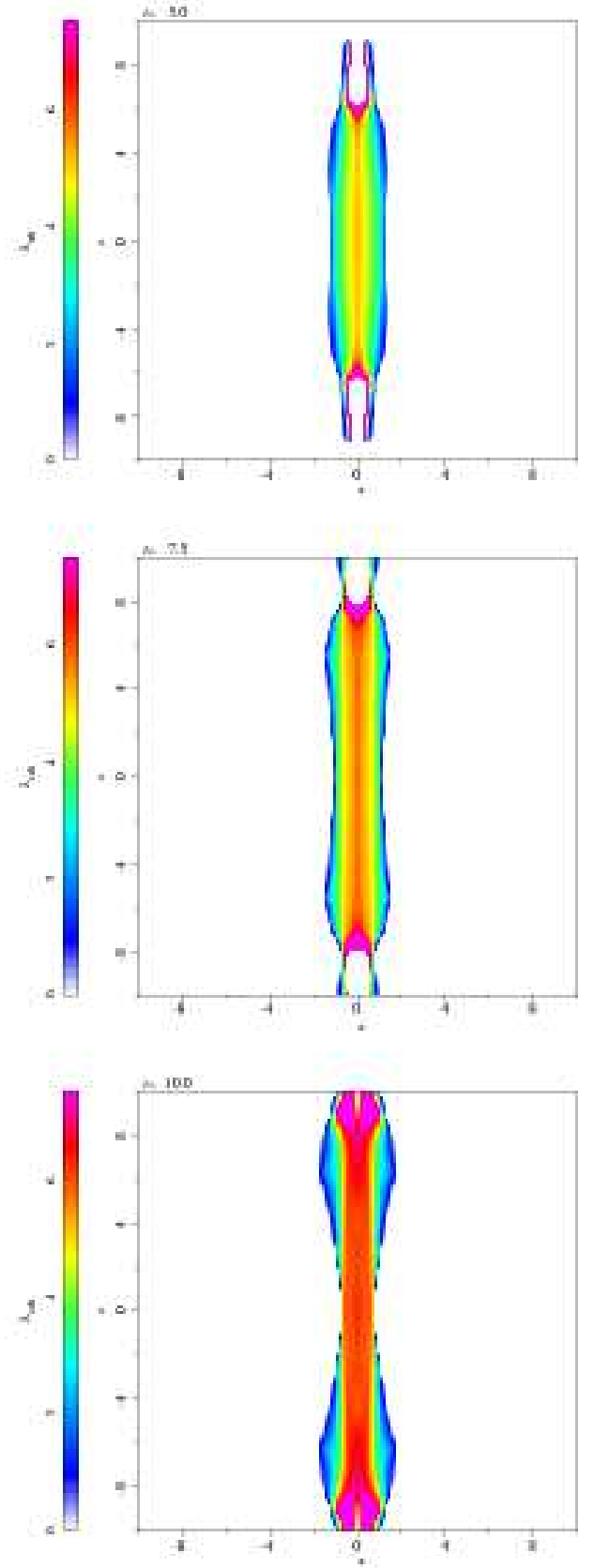


FIG. 4.— Time evolution of the K-S critical wavelength λ_{crit} in the $x - z$ plane at $t = 5.0$ (*Top*), 7.5 (*Middle*), and 10.0 (*Bottom*) in the unperturbed case (Paper II).

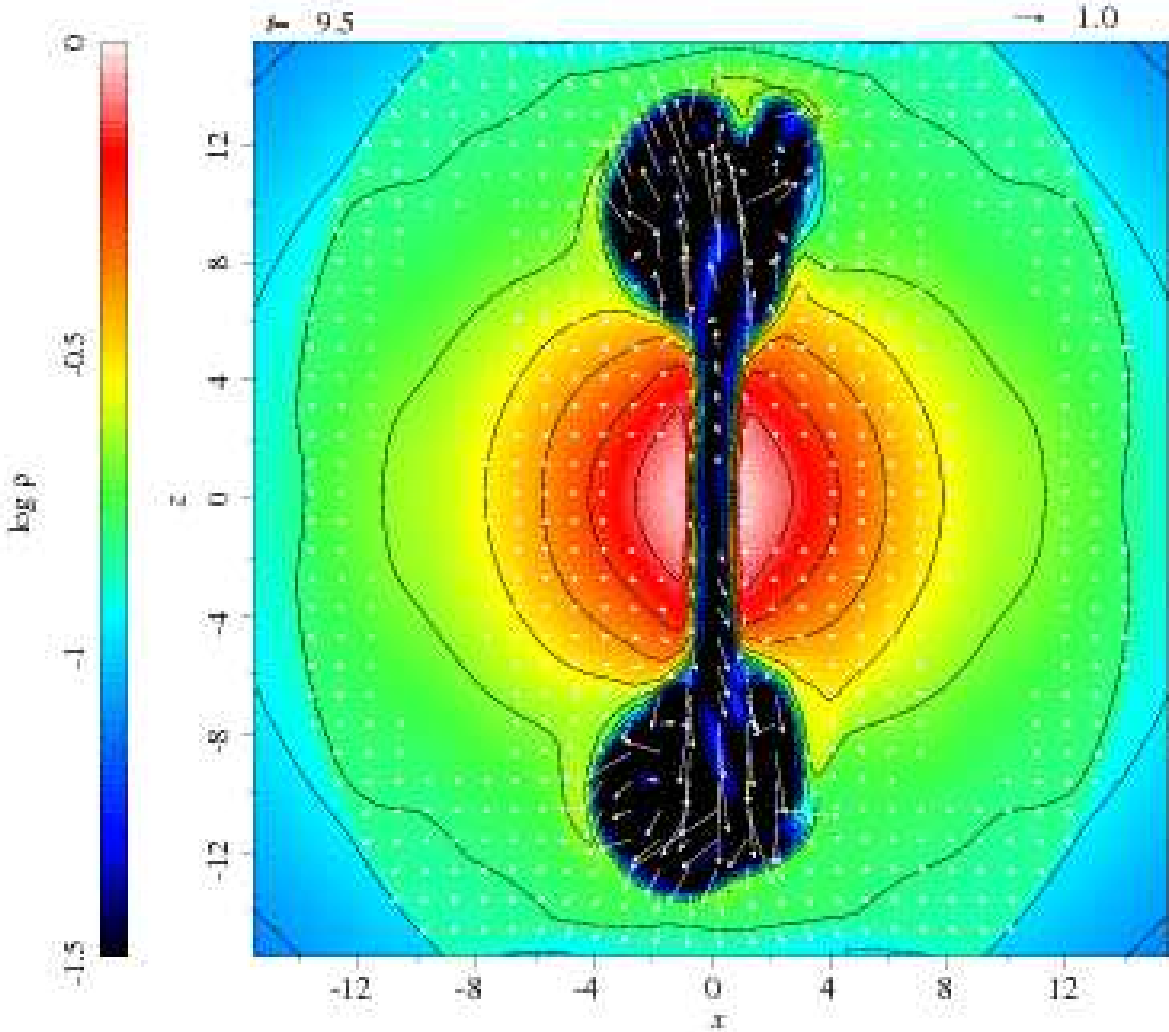


FIG. 5.— Distribution of the density ρ (logarithmic scale) in the $x - z$ plane is shown along with the poloidal velocity field (arrows) at $t = 9.5$ in the perturbed case. Similar to the unperturbed case (Paper II), density cavities are formed due to the magnetic field expansion, while the non-axisymmetric motion can be seen. The length of the arrow at the upper right shows the unit speed.

and e corresponds to the external medium). On the other hand, the non-axisymmetric “body” (internal) modes ($m > 1$) can become important and affect the jet interior in the following situations: (1) if the jet velocity exceeds the super-fast magnetosonic speed V_f :

$$V_j > V_f, \quad (13)$$

or (2) if the flow velocity is slightly below the slow magnetosonic speed V_s :

$$\frac{C_s V_A}{\sqrt{C_s^2 + V_A^2}} < V_j < V_s, \quad (14)$$

where C_s is the sound speed and V_A is the Alfvén speed (Hardee & Rosen 1999).

Figure 10 shows the transverse profiles in the x direction of several quantities at $t = 8.0$ in the perturbed case. Two different axial positions $z = 2.0$ and 8.0 are selected for examining the KHI surface/body modes. For the surface modes, we inspect the transverse distribution of the bulk flow speed V , the density ρ , and the magnetic field strength B . Two distinct velocity shears (in both positive and negative x regions) are identified in the x direction on $z = 2.0$ (*upper-left*); an outer part $0.6 \lesssim |x| \lesssim 1.5$ and an inner part $0.2 \lesssim |x| \lesssim 0.6$.

At the outer part, $\Delta V \sim 1.2$ and $V_{As} \sim 1.8$ and at the inner part, $\Delta V \sim 1.1$ and $V_{As} \sim 8.7$. Therefore, the inequality $\Delta V < V_{As}$ is satisfied. Similarly, we can see many distinct velocity shears in the *upper-right* panel. However, even in these shears, we confirm that the inequality $\Delta V < V_{As}$ still holds everywhere. This indicates that the KHI surface modes are completely stabilized, because there is no significant velocity shear exceeding the local surface Alfvén speed in the transverse (x) direction. For the body modes, we inspect the transverse distribution of the bulk flow speed V , the Alfvén speed, and the quantity $C_s V_A / (C_s^2 + V_A^2)^{1/2}$. Inside the magnetic tower, the plasma β ($= 2p/B^2$) is always less than unity during the time evolution. Therefore, the phase speed of the MHD fast mode wave is equal (in the local magnetic field direction) or larger (in the oblique direction of the local magnetic field) than the Alfvén speed, $V_f \geq V_A$. As seen in both *Bottom* panels in Fig. 10, the bulk flow speed is always extremely sub-Alfvénic, and furthermore, the inequality $V < C_s V_A / (C_s^2 + V_A^2)^{1/2}$ is also satisfied in the “body” part of the magnetic tower jet. These indicate that the KHI body modes are suppressed as well. We conclude that the KHI modes play no role and the normal CDI modes create the non-axisymmetric structures in our results.

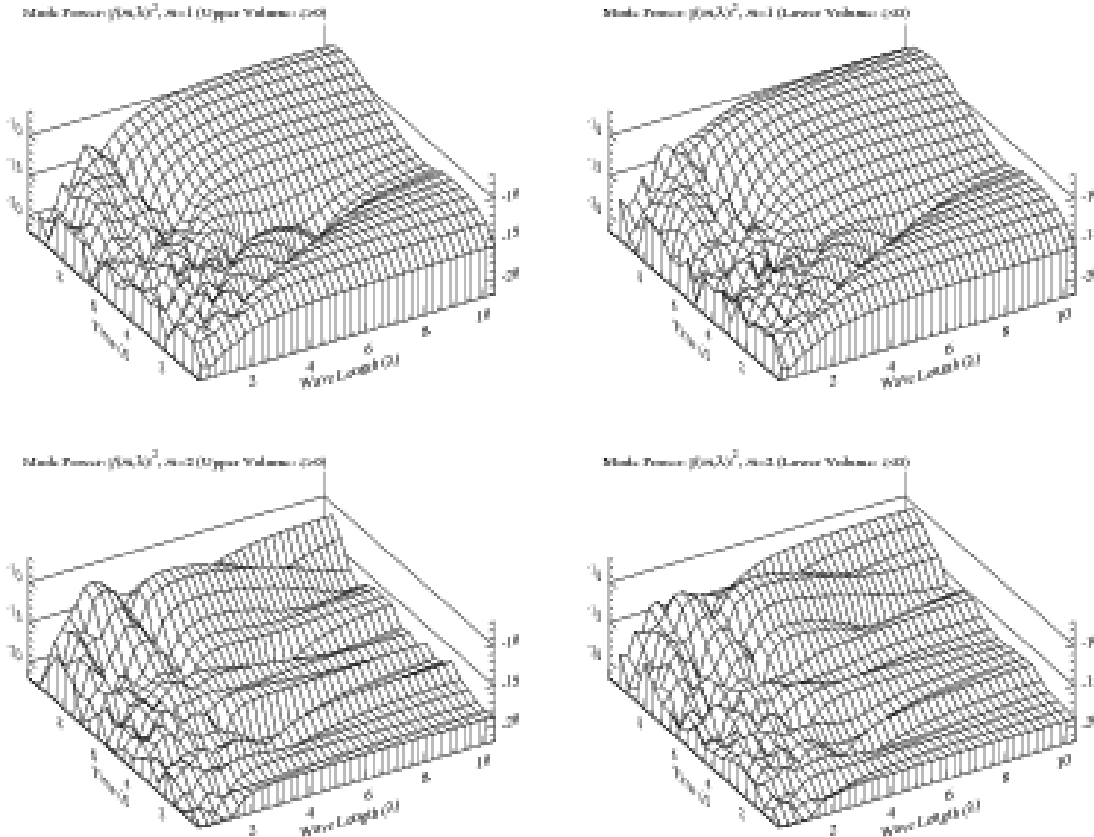


FIG. 6.— Similar to Fig. 2, but for modes $m = 1$ (Top) and 2 (Bottom) in the perturbed case. Left: For the upper volume $z > 0$. Right: For the lower volume $z < 0$.

4.2. Stabilization/Destabilization of Magnetic Tower Jets

As examined in §3.1, the unperturbed magnetic tower jet can be stabilized against the CDI kink mode beyond the K-S criterion. One of the certain mechanisms of the stabilizing effect, which we can identify in our unperturbed case, is the dynamical relaxation of magnetic twists. However, this process may contribute the *marginal stabilization* under an ideal situation (no perturbation except for the numerical noise is assumed as an initial condition). If the system is perturbed randomly with a finite amplitude (a few percent of the local sound speed), then the non-axisymmetric ($m \geq 1$) internal/external CDI modes can grow. The disturbances in the system are reasonable (especially when related to possible astrophysical situations). Therefore, the magnetic tower jet in our treatments, will eventually be subject to CDI. Here, we give further discussions on the stabilities of magnetic tower jets.

4.2.1. Line-tying Effect

In the solar coronal magnetic loops, it is well known that the line-tying effect at the foot points (chromosphere) can raise the original K-S stability threshold (dense materials can prevent the radial motion of twisted magnetic fluxes). How about the case in the astrophysical jets? Anchored magnetic fluxes to the accretion disk and/or stellar/black hole surfaces may be considered as a semi (one side) line-tying boundary condition in a certain dynamical stage. An important clue to this can be derived from laboratory experiments of magnetic towers (Hsu & Bellan 2002, 2003). Their quasi “force-free” magnetic towers can exhibit the systematic $m = 1$ distortion when the current-carrying system satisfies the original K-S limit. It might be unlikely that such a semi line-tying effect can stabi-

lize the jet even in the astrophysical situation. In our global modeling of magnetic tower jets, we do not solve the evolution of the central region (an accretion disk, etc.). Therefore, we can not apply it directly to the AGN central region. It is still an open issue whether a semi line-tying effect can work or not in the real astrophysical jets.

4.2.2. Internal Thermal Pressure

As discussed in Paper II, the “forward” current-carrying column \mathbf{J}^F never reaches a force-free equilibrium. Instead, it will be supported by the outward-directed, local (core of the magnetic towers) pressure gradient force: $-\nabla p + \mathbf{J} \times \mathbf{B} \simeq 0$ during a dynamical evolution (see Fig. 10 in Paper II). In terms of minimization of the MHD energy integral (Bernstein et al. 1958), a finite gas pressure in the system (plasma $\beta \neq 0$) can contribute to the stabilization. However this can be effective when $\beta \gtrsim 1$, i.e., the gas pressure is more dominant than the magnetic pressure (for $m = 1$ kink mode, see Hood & Priest 1979). Therefore, we may not expect a strong stabilization by the pressure in the magnetic tower ($\beta \lesssim 0.1$). Furthermore, the outward-directed gas pressure gradient itself ($-\nabla p > 0$) actually destabilizes the tower through the PDI (interchange and/or ballooning) modes, which is driven by the perpendicular currents (in contrast to the axial [parallel] currents, considered mainly in this paper). We, however, could not find any growth of the PDI modes, in both the unperturbed (Paper II) and the perturbed cases, implying no direct contribution of the pressure gradient to the destabilization by the PDI modes (see next section for more details). Also, we can not confirm any direct contributions of the internal thermal pressure effects ($\beta \neq 0$ and $-\nabla p$)

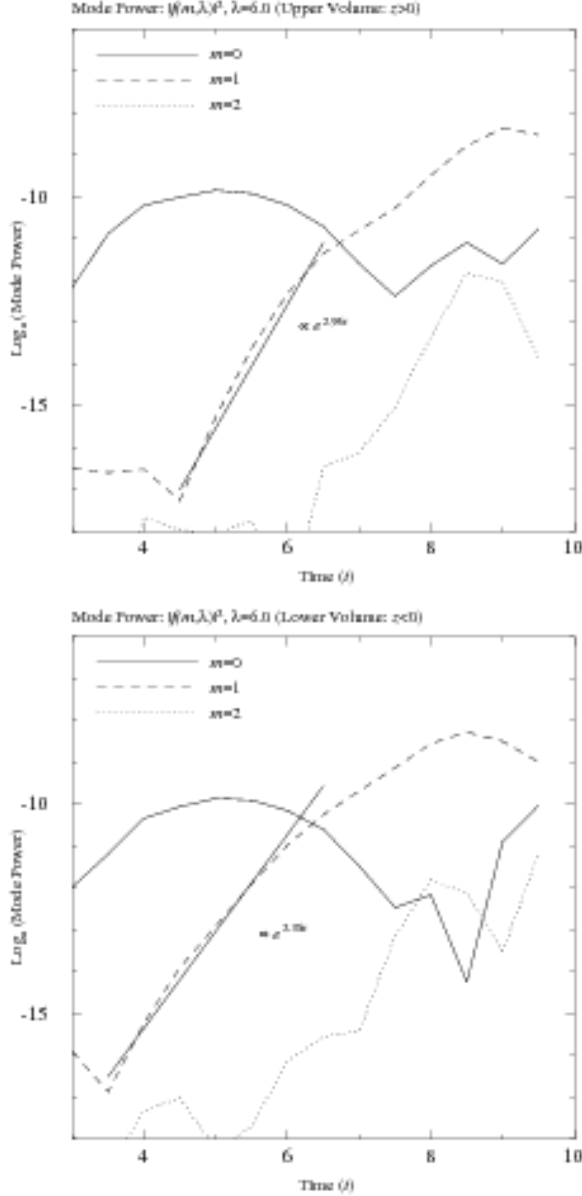


FIG. 7.— Similar to Fig. 3, but for modes $m = 0 - 2$ in the perturbed case. Straight lines are derived by fitting the slopes of the $m = 1$ mode growth to a linear function. *Top*: For the upper volume $z > 0$. *Bottom*: For the lower volume $z < 0$.

to the destabilization by the CDI internal/external modes.

4.2.3. Magnetic Field Configuration

We next consider the magnetic field configuration in magnetic tower jets. In the context of magnetic controlled fusion systems, the helical field configuration in the tower model can be identified as the reversed field pinch (RFP) profile as seen in Fig. 11 in Paper II. The axial component B_z has a crucial shear (its sign reverses from “+” to “-”) in the radial direction (RFP in the context of astrophysical jets, see also Benford 2006). Several stabilization effects in RFP are summarized in Freidberg (1982); (i) a hollow or very flat pressure profile ($\nabla p \simeq 0$) are required near the central (z) axis to suppress the PDI sausage (interchange, internal) mode ($m = 0$), but (ii) it can be suppressed when $\beta \lesssim 0.5$. This may be the situation in the present paper. As already discussed in the previous section (§4.2.2), a finite pressure gradient exists to contribute to

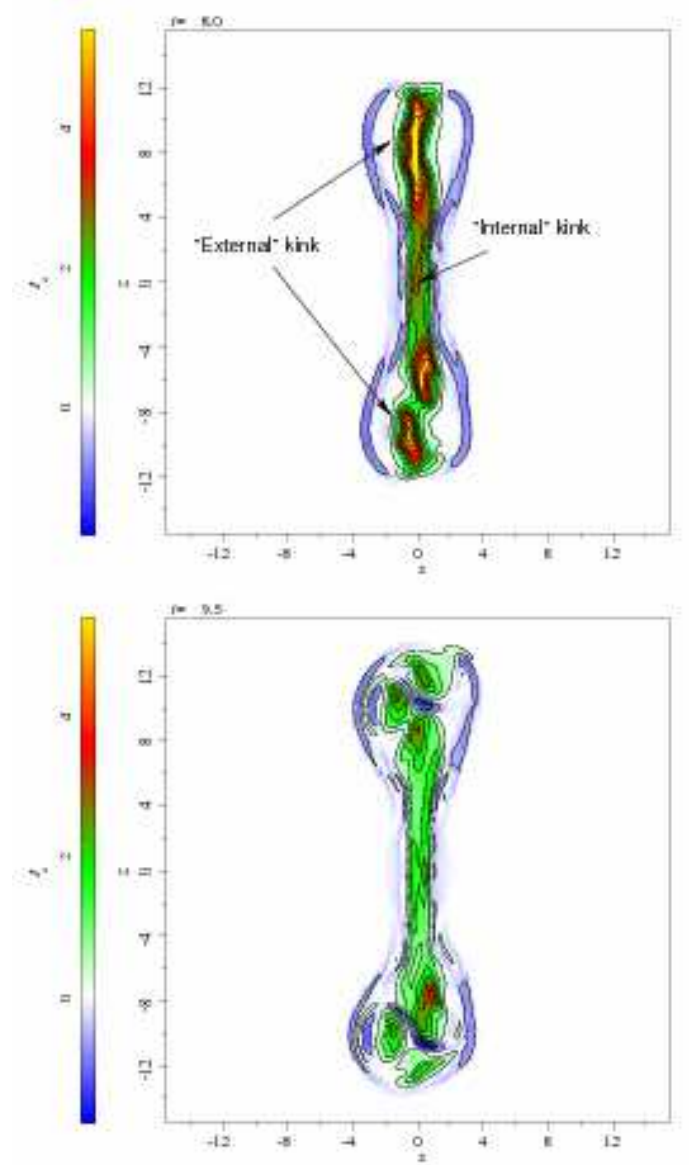


FIG. 8.— Snapshots of the axial current density J_z in the $x - z$ plane at $t = 8.0$ (*Top*) and 9.5 (*Bottom*) in the perturbed case. Two types of growing kink modes (“External”/“Internal”) are illustrated on the *Top* panel.

the radial force equilibrium in the core part (around the central axis) and this might play a role in driving the PDI modes. However, the plasma β is small ($\beta \lesssim 0.1$), indicating that the destabilization by the PDI modes may be suppressed due to the small plasma β . Also, (iii) the strong B_z shear can prevent the destabilization by the CDI internal/external kink modes ($m = 1$). In our results, this shear may provide the stabilization against the CDI external modes, while it does not affect the CDI internal modes at the lower latitude $|z| \lesssim 4$, as seen in Figs. 6 and 8. Furthermore, the CDI external modes can grow at the higher latitude $|z| \gtrsim 4$. This may be because the strong B_z shear in the radial direction will be relaxed towards the jet axis due to the decreasing external pressure (expanding the poloidal fluxes to the radial direction).

4.2.4. External Environment

The external gas itself also may affect the stabilization. The inward-directed, thermal pressure confinement and/or

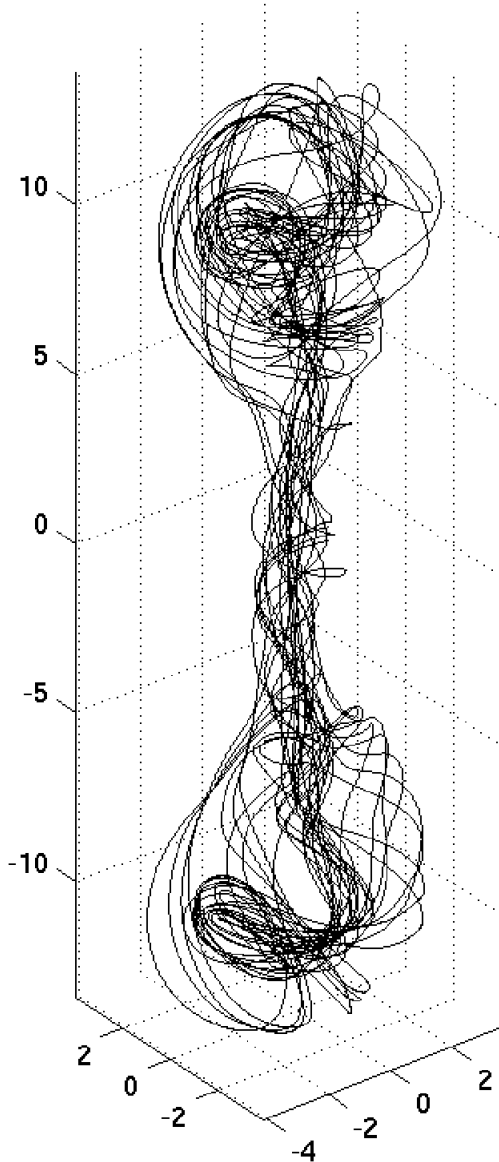


FIG. 9.— Three-dimensional view of some selected magnetic lines at $t = 9.5$ in the perturbed case.

the gravitational contraction of the external unmagnetized gas, which surrounds the magnetic tower jets, may provide some stabilization at least against the growth of external CDI modes, although the internal CDI and PDI modes will not be affected (for the internal PDI sausage $m = 0$ mode, see Lery & Frank 2000). In our results, the external environment may have a similar stabilizing effect on the external CDI modes to the B_z shear, as discussed in the previous section (§4.2.3), while the internal PDI mode may be suppressed by the low internal pressure. In the magnetic tower jets, an external gas plays a crucial role in the stabilization of the CDI external modes. When an external gas pressure profile does not decrease (constant), which is examined in Paper I (see Fig. 11 in Paper I for a continuous injection case), the magnetic tower never expands radially and both the thermal confinement by the external gas and the strong B_z shear will be kept throughout the magnetic tower “body” (no formation of “lobe”). Therefore, the CDI internal modes may occur,

but the CDI external modes should be suppressed. These are consistent with the CDI “non-disrupting” model (Appl 1996; Appl et al. 2000; Lery et al. 2000) as well.

4.2.5. Rotation

We finally discuss the stabilization by the rotation. In our numerical treatment, we investigate almost “non-spinning” magnetic tower jet. From the theoretical point of view, any magnetically driven outflows (magneto-centrifugal and/or magnetic pressure driven) can have an azimuthal velocity component. They possess an angular momentum provided by the accretion disk or Kerr black hole magnetosphere. In the classical model of nonrelativistic MHD winds, the centrifugal force plays a minor role in the radial force equilibrium far from the accretion disk (Blandford & Payne 1982). However, this is only the case in the nonrelativistic treatment. In the relativistic MHD regime, the situation will be modified; semi-analytical solutions of relativistic MHD winds with self-similarity exhibit that the relativistic inertia and electrostatic forces play an important role in the radial force equilibrium at the cylindrical flow structure, extended to pc or larger scales (Vlahakis & Königl 2003). Braided emission-line profiles and rotational velocity in NGC 4258 indicate a pure helical motion exists along the tightly wrapped strand even in kpc scales (Cecil, Wilson, & Tully 1992).

The stabilizing effect of rotation against the CDI kink mode in the spinning nonrelativistic PFD/KFD jets has been investigated by numerical simulations (Nakamura & Meier 2004). Because of the centrifugal effect, these spinning jets can be stabilized against the $m = 1$ mode beyond the point predicted by the K-S criterion. The linear stability analysis of the relativistically rotating force-free fields in Kerr geometry (Blandford & Znajek 1977) has been performed by Tomimatsu, Matsuoka, & Takahashi (2001). They also show that the field-line rotation has a stabilizing effect against the kink modes satisfying the K-S criterion. In these cases, the presence of an azimuthal velocity component can modify the radial force equilibrium, making the jet robust against the CDI kink mode. Examinations of the stability property in a rotating magnetic tower jet are clearly desirable.

4.3. External CDI Kink Mode as a Possible Mechanism for Wiggling AGN Jets

The CDI of current-carrying jets for two types of return current distributions have been discussed: (1) the return current is assumed to flow within the jet itself (the jets are thermally confined by the external medium) (Chiuderi, Pietrini, & Torricelli-Ciamponi 1989), and (2) the return current is assumed to flow around the jet, such as in a magnetized cocoon (Benford 1978, 2006). Most of the theoretical/numerical works have been devoted to the former case, in which the forward current \mathbf{J}^F and the return current \mathbf{J}^R are concentrated at the interfaces between the jet and ISM/IGM, which is taken to be “unmagnetized”. In this situation, the growth of external CDI modes can be effectively suppressed, while the excitations of only internal CDI modes are allowed. There is no radial displacement at the edge of the current-carrying column by the internal CDI modes, and therefore, it may be difficult to explain the off-set axial distortion of observed jets by these internal modes. As described in §1, this is one of the reasons why much less attention has been paid to the CDI than to the KHI for the stability problems in astrophysical jets to explain the disrupted jet exterior.

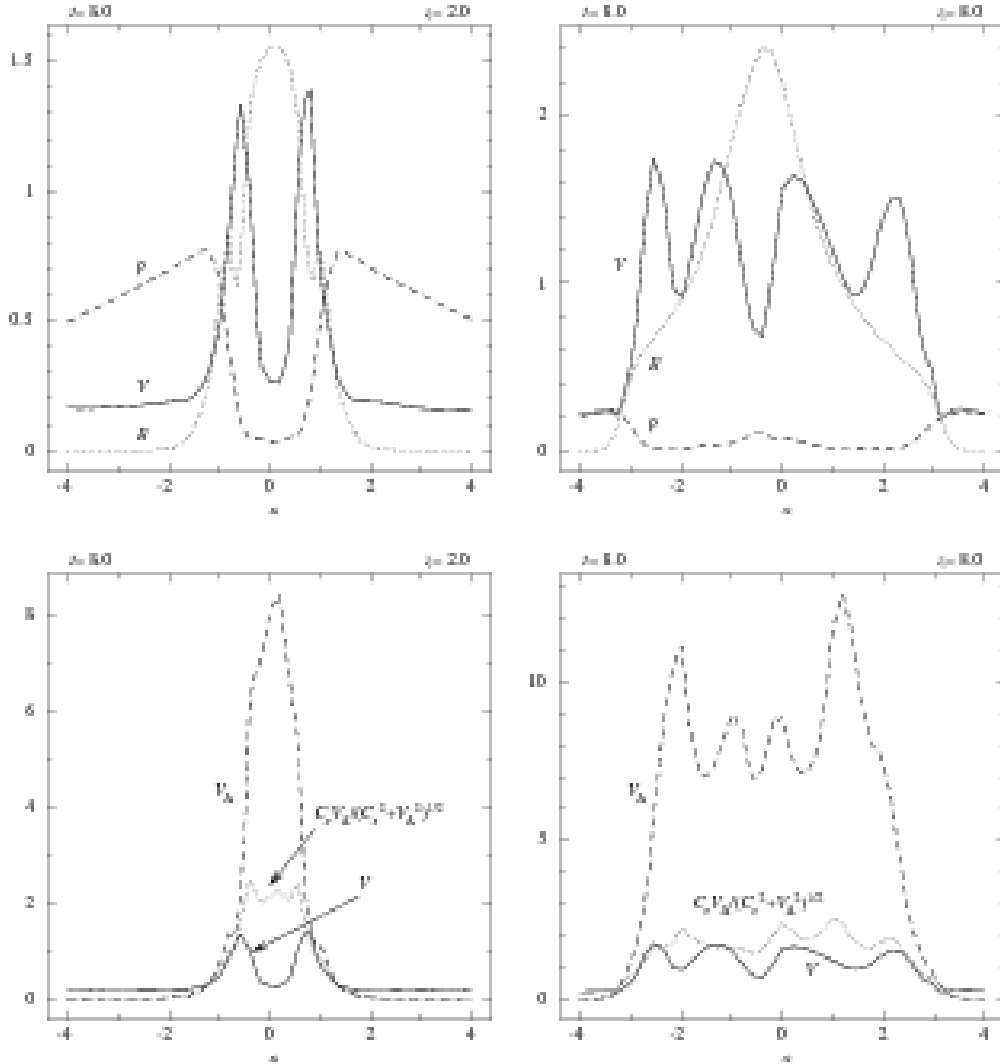


FIG. 10.— Transverse profiles in the x direction of several quantities at $t = 8.0$ on $z = 2.0$ (Left panels) and on $z = 8.0$ (Right panels) in the perturbed case. The bulk speed V ($= \sqrt{V_x^2 + V_y^2 + V_z^2}$), the density ρ , and the magnetic field strength B ($= \sqrt{B_x^2 + B_y^2 + B_z^2}$) are shown for inspecting the KHI surface modes (Top panels). The bulk speed V , the Alfvén speed V_A , and the quantity $C_s V_A / (C_s^2 + V_A^2)^{1/2}$ are shown for inspecting the KHI body modes (Bottom panels).

However, in the gravitationally stratified atmosphere, the effect of thermal confinement on the edge of the current-carrying column will get gradually weaker as the magnetic tower grows. As a result, a separation of current flowing paths between \mathbf{J}^F and \mathbf{J}^R occurs, as seen in Fig. 8. This implies that the edge of \mathbf{J}^F becomes a free boundary against the CDI external modes, even when it is embedded deeply inside the external, unmagnetized gas. Furthermore, the region between the outside of \mathbf{J}^F and the inside of \mathbf{J}^R becomes nearly force-free $\mathbf{J} \times \mathbf{B} \simeq 0$. Therefore, the CDI external modes can grow in a dynamical time scale to form the systematic wiggles. This is also true even in the spinning PFD/KFD jets under the large-scale magnetic field (Nakamura et al. 2001; Nakamura & Meier 2004). On the other hand, even if the gas pressure in the external, unmagnetized gas is high enough to suppress the growth of the CDI external kink mode, then the CDI internal kink mode can grow to form the internal non-axisymmetric structure, as we exhibited in Fig. 8. Therefore, we believe that the external CDI modes are one of the possible mechanisms to explain the disruption of current-carrying MHD jets and it could be applied to the wiggling AGN jets.

5. CONCLUSION

Stability properties of magnetic tower jets have been examined by performing 3-D MHD simulations. Our numerical results show that the magnetic tower jets in the gravitationally stratified atmosphere could survive the current-driven kink instability beyond the Kruskal-Shafranov criterion even in the nonlinear regime. One of the potentially stabilizing effects on a traditionally unstable magnetic field may be due to the dynamical relaxation of magnetic twists in the propagating magnetic tower jets. This causes an increased threshold of the unstable critical wavelength.

However, the magnetic tower jets are eventually distorted by the non-axisymmetric perturbations with a few percent of the local sound speed in the system. The current-driven kink modes grow predominantly on time scales of the order of the local Alfvén crossing time τ_A . In the gravitationally stratified atmosphere, two types of kink modes appears: the internal and external modes. At a large distance away from the central region, the external kink mode grows, while only the internal kink mode exhibits near the central region. Therefore, the exterior of magnetic tower jets will be deformed into a large-

scale wiggled structure by the external kink mode.

Possible mechanisms of stabilizing/destabilizing in the magnetic tower jets under the gravitationally stratified atmospheres are discussed. None of the growing surface/body modes of Kelvin-Helmholtz instability are identified due to the small velocity shear and slow bulk speed (compared with the local Alfvén speed). The pressure-driven instabilities are also inhibited due to the low plasma β ($\lesssim 0.1$) inside the magnetic towers. The “reversed field pinch” field configuration in the towers and the external unmagnetized gas may provide some stabilization effects on the current-driven external modes.

Non-axisymmetric current-driven instabilities ($m \geq 1$) are absolute instabilities, i.e., they grow but do not propagate in the jet co-moving (rest) frame (Appl et al. 2000; Nakamura & Meier 2004). If the dissipation timescale τ_d of the current associated with jets is much longer than the jet

dynamical timescale $\tau_j \lesssim \tau_A \sim \tau_{\text{CDI}} \ll \tau_d$, the patterns created by the CDI modes will persist for some time as the flow advances. And the bulk flow itself will appear to travel in a true 3-D helical pattern as it follows the magnetic backbone of the helix, as observationally expected in several radio sources as 3C 345 (Zensus et al. 1995), 3C 120 (Gomez et al. 2001), and 3C 449 (Feretti et al. 1999).

Helpful discussions with J. Finn are gratefully acknowledged. This work was carried out under the auspices of the National Nuclear Security Administration of the U.S. Department of Energy at Los Alamos National Laboratory under Contract No. DE-AC52-06NA25396. It was supported by the Laboratory Directed Research and Development Program at LANL and by IGPP at LANL.

REFERENCES

- Appl, S., & Camenzind, M. 1992, *A&A*, 256, 354
 Appl, S. 1996, *A&A*, 314, 995
 Appl, S., Lery, T., & Baty, H. 2000, *A&A*, 355, 818
 Bateman, G. 1978, *MHD Instabilities* (Cambridge: MIT Press)
 Baty, H., & Keppens, R. 2002, *ApJ*, 580, 800
 Baum, S. A., et al. 1997, *ApJ*, 483, 178
 Begelman, M. C., Blandford, R. D., & Rees, M. J. 1980, *Nature*, 287, 307
 Begelman, M. C. 1998, *ApJ*, 493, 291
 Benford, G. 1978, *MNRAS*, 183, 29
 Benford, G. 2006, *MNRAS*, 369, 77
 Bernstein, I. B., Frieman, E. A., Kruskal, M. D., & Kulsrud, R. M. 1958, *Proc. R. Soc. London, Ser. A* 244, 17
 Blandford, R. D., & Payne, D. G. 1982, *MNRAS*, 199, 883
 Blandford, R. D., & Znajek, R. L. 1977, *MNRAS*, 179, 433
 Bodo, G., Rosner, R., Ferrari, A., & Knobloch, E. 1989, *ApJ*, 341, 631
 Cecil, G., Wilson, A. S., & Tully, R. B. 1992, *ApJ*, 390, 365
 Chiuderi, C., Pietrini, P., & Torricelli-Ciamponi, G. 1989, *ApJ*, 339, 70
 Eichler, D. 1993, *ApJ*, 419, 111
 Eilek, J. A., & Owen, F. N. 2002, *ApJ*, 567, 202
 Einaudi, G., & Van Hoven, G. 1983, *Sol. Phys.*, 88, 163
 Feretti, L., Perley, R., Giovannini, G., & Andernach, H. 1999, *A&A*, 341, 29
 Frank, A., Lery, T., Gardiner, T. A., Jones, T. W., & Ryu, D. 2000, *ApJ*, 540, 342
 Freidberg J. P. 1982, *Rev. Mod. Phys.*, 54, 801
 Gomez, J-L., Marscher, A.P., Alberdi, A., Jorstad, S.G., & Agudo, I. 2001, *ApJ*, 561, L161
 Hardee, P. E., & Rosen, A. 1999, *ApJ*, 524, 650
 Hardee, P. E., & Rosen, A. 2002, *ApJ*, 576, 204
 Hardee, P. E. (2004), *Ap&SS*, 293, 117
 Hood, A. W., & Priest, E. R. 1979, *Sol. Phys.*, 64, 303
 Hsu, S. C., & Bellan, P. M. 2002, *MNRAS*, 334, 257
 Hsu, S. C., & Bellan, P. M. 2003, *Phys. Rev. Lett.*, 90, 215002
 Hummel, C. A., et al. 1992, *A&A*, 257, 489
 Istomin, Ya. N., & Pariev, V. I. 1994, *MNRAS*, 267, 629
 Istomin, Ya. N., & Pariev, V. I. 1996, *MNRAS*, 281, 1
 Kadomtsev, B. B., 1966, *Rev. Plasma Phys.*, 2, 153
 Kigure, H., Uchida, Y., Nakamura, M., Hirose, S., & Cameron, R. 2004, *ApJ*, 608, 119
 King, I. 1962, *AJ*, 67, 471
 Kruskal, M. D., Johnson, J. L., Gottlieb, M. B., & Goldman, L. M. 1958, *Phys. Fluids*, 1, 421
 Kudoh, T., & Shibata, K. 1997, *ApJ*, 474, 362
 Lery, T., Baty, H., & Appl, S. 2000, *A&A*, 355, 1201
 Lery, T., & Frank, A. 2000, *ApJ*, 533, 897
 Li, H., Lapenta, G., Finn, J. M., Li, S., & Colgate, S. A. 2006, *ApJ*, 643, 92 (Paper I)
 Lobanov, A. P., & Zensus, J. A. 2001, *Science*, 294, 128
 Lyubarskii, Yu. E. 1999, *MNRAS*, 308, 1006
 Nakamura, M., Uchida, Y., & Hirose, S. 2001, *New Astronomy*, 6, 61
 Nakamura, M., & Meier, D. L. 2004, *ApJ*, 617, 123
 Nakamura, M., Li, H., & Li, S. 2006, accepted for publication in *ApJ*; preprint (astro-ph/0608326) (Paper II)
 Marshall, H. L., et al. 2001, *ApJ*, 549, L167
 Meier, D. L., Koide, S., & Uchida, Y. 2001, *Science*, 291, 84
 Reid, M. J., Biretta, J. A., Junor, W., Muxlow, T. W. B., & Spencer, R. E. 1989, *ApJ*, 336, 112
 Savolainen, T., Wiik, K., Valtaoja, E., & Tornikoski, M. 2006, *A&A*, 446, 71
 Shafranov, V. D. 1957, *Sov. Phys.-JETP*, 6, 545
 Spruit, H. C., Foglizzo, T., & Stehle, R. 1997, *MNRAS*, 288, 333
 Todo, Y., Uchida, Y., Sato, T., & Rosner, R. 1993, *ApJ*, 403, 164
 Tomimatsu, A., Matsuoka, T., & Takahashi, M. 2001, *Phys. Rev. D*, 64, 123003
 Vlahakis, N., Tsinganos, K., Sauty, C., & Trussoni, E. 2000, *MNRAS*, 318, 417
 Vlahakis, N., & Königl, A. 2001, *ApJ*, 563, L129
 Vlahakis, N., & Königl, A. 2003, *ApJ*, 596, 1080
 Zensus, J.A., Cohen, M.H., & Unwin, S.C. 1995, *ApJ*, 443, 35